Journal of Innovative Optical Health Sciences
Vol. 13, No. 3 (2020) 2040001 (9 pages)

DOI: 10.1142/S1793545820400015

World Scientific
www.worldscientific.com

Simplifying the detection of optical distortions by machine learning

Shuwen Hu[*,†], Lejia Hu[*,†], Biwei Zhang[*,†], Wei Gong[‡,§] and Ke Si[*,†,‡,¶]

[*]*State Key Laboratory of Modern Optical Instrumentation*
Department of Neurobiology of the First Affiliated Hospital
Zhejiang University School of Medicine
Hangzhou 310027, P. R. China

[†]*College of Optical Science and Engineering*
Zhejiang University
Hangzhou 310027, P. R. China

[‡]*Center for Neuroscience*
Department of Neurobiology
NHC and CAMS Key Laboratory of Medical Neurobiology
Zhejiang University School of Medicine
Hangzhou 310058, P. R. China
[§]*weigong@zju.edu.cn*
[¶]*kesi@zju.edu.cn*

Received 7 July 2019
Accepted 14 October 2019
Published 26 November 2019

Adaptive optics has been widely used in biological science to recover high-resolution optical image deep into the tissue, where optical distortion detection with high speed and accuracy is strongly required. Here, we introduce convolutional neural networks, one of the most popular machine learning models, into Shack–Hartmann wavefront sensor (SHWS) to simplify optical distortion detection processes. Without image segmentation or centroid positioning algorithm, the trained network could estimate up to 36th Zernike mode coefficients directly from a full SHWS image within 1.227 ms on a personal computer, and achieves prediction accuracy up to 97.4%. The simulation results show that the average root mean squared error in phase residuals of our method is 75.64% lower than that with the modal-based SHWS method. With the high detection accuracy and simplified detection processes, this work has the potential to be applied in wavefront sensor-based adaptive optics for *in vivo* deep tissue imaging.

Keywords: Machine learning; adaptive optics; wavefront sensor.

[§,¶]Corresponding authors.

1. Introduction

Optical microscopy has become an essential tool for various applications in biological science.[1,2] However, due to the optical properties of the specimen, such as the refractive index varies with time and space, the unwanted optical distortions are induced. Not only the spatial resolution but also the contrast of microscope images is degraded by the induced distortion, which limits the effective imaging depth of the microscope.

To improve the imaging performance of the microscope, adaptive optics (AO) is used to measure and then compensate the optical distortions. The commonly chosen strategy is to utilize direct wavefront sensing methods, such as Shack–Hartmann wavefront sensor (SHWS).[3] Combining with suitable guide stars, SHWS has been applied in ocular aberration detection and deep tissue morphological or functional imaging.[1,4–8] Another approach to compensate the optical distortion is to use indirect wavefront sensing methods, such as coherent adaptive optical technique (COAT), which has been applied in optical focusing, biological imaging and optogenetics.[9–11] However, COAT has to modulate the incident wavefront to optimize the focal intensity, which limits its detection speed. Compared with indirect wavefront sensing methods, the high optical distortions measuring speed of SHWS enables the improvement of imaging quality in real-time biological imaging.

Although SHWS has a high distortion detection speed, its processes are quite complex, which are closely related to image processing.[12] Before the measurement, an ideal spot pattern (without distortion) for reference is recorded first. When the sensor receives a distorted wavefront, the distortion causes wavefront slopes over each micro-lens, which results in the displacement of each focal spot on the sensor. The displacement between each spot and the ideal spot is related to the wavefront's local tilt over each micro-lens. In order to reconstruct the optical distortions under detection, the distorted spot pattern will be recorded to calculate the centroid of each spot. The position of each centroid is used to compute the displacement of each spot in x- and y-directions. At last, the optical distortions are reconstructed by the calculated local derivatives through zonal or modal approaches.

The complex processes of optical distortions detection somehow limit the application potential of SHWS. Several works have been reported to speed up the implementation of the process.[12,13] However, the hardware upgrades and the complex processes above are still inevitable. Besides, the SHWS utilizes approximation during the wavefront reconstruction, where the average wavefront slopes are used to calculate the wavefront while the information in the intensity distribution of the spots still remain unutilized.

Recently, machine learning or deep learning has become a powerful tool to improve the imaging performance of the microscope.[14–17] In the field of AO or wavefront sensing, several works have been proposed to overcome the light scattering or implement phase retrieval using machine learning-based methods.[18–21] Although these methods could directly estimate the distortion by inputting a distorted point spread function (PSF), it is hard to capture the effective PSFs in the biological imaging. As for the SHWS, artificial neural networks have been reported to reconstruct the wavefront or improve the centroid positioning accuracy.[22,23] However, they still need to calculate the spot displacements or the derivatives of the wavefront for distortion detection. The optical distortion detection processes of SHWS still remain to be simplified.

In this paper, we report a new approach based on machine learning to measure the optical distortions. Our method utilizes a similar strategy to the modal-based SHWS approach, which uses the Zernike polynomials to fit the optical distortions under detection. The proposed method simplifies the optical distortions detection processes, which eliminates several steps, such as centroid positioning, image segmentation, centroid displacement calculation and local derivative solving. With a full spot pattern from SHWS inputted, the trained model could output the corresponding Zernike mode coefficients with a high speed. The prediction accuracy and the mean squared error (MSE) of the predicted mode coefficients are quantitatively evaluated using amounts of datasets. The performance of this method, including optical distortions prediction and distorted focus recovery, is presented and compared with modal-based approach through simulations.

2. Simulation and Methods

In order to validate the concept of our method and quantitatively evaluate its wavefront detection

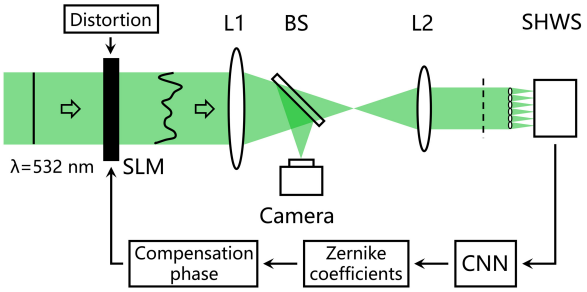

Fig. 1. The schematics of the simulation system setup. L1–L2, lens; BS, nonpolarizing beam splitter. The black solid line indicates the wavefront of the incident beam and the black dotted line indicates the rear pupil plane of the micro-lens array.

accuracy, we simulated a SHWS to obtain the spot patterns for machine learning model training. The simulation system setup is illustrated in Fig. 1. A laser with 532nm wavelength was used as the light source. A spatial light modulator (SLM) served as the distortion generator as well as the wavefront compensator. The incident light beam with distorted wavefront was focused by a lens and separated into two parts. One part of the light was captured by a camera, which was used to monitor the focusing quality. the other part was collected by another lens to form distorted spot array pattern on the SHWS. The rear pupil plane of the micro-lens array was conjugated with the SLM to ensure the wavefront sensing reliability. The micro-lens array contains 12×12 subapertures and around 120 micro-lenses were used in the simulation.

Here, we used a summation of the Zernike polynomials to describe the distortions in the neural network training and testing, which is a set of basis functions that are orthogonal within a unit circle.[24] In this case, the optical distortion can be mathematically described as follows:

$$\varphi(x, y) = \sum_{n=0}^{\infty} a_n Z_n(x, y), \tag{1}$$

where $\varphi(x, y)$ is the wavefront distribution inside a unit circle, a_n is the nth Zernike mode coefficient and $Z_n(x, y)$ is the nth Zernike basis function. Fourier shift theorem was used to simulate the wavefront propagation and generate the SHWS patterns. Each set of coefficients corresponds to a SHWS pattern uniquely. In this paper, up to 36th Zernike mode coefficients were used to generate 32,768 training datasets, 10,240 validation datasets and 4096 testing datasets for obtaining the corresponding distortion pattern on the SHWS. In order to evaluate the performance of our model, another 1024 datasets were generated for repeatability verification. Table 1 gives the coefficient ranges of corresponding Zernike modes.

Before training the network, the SHWS patterns were downsampled to size 192×192. Then they were standardized using min–max normalization:

$$x_i = \frac{I_i - \min(I_i)}{\max(I_i) - \min(I_i)}, \tag{2}$$

where I_i is the ith original intensity distribution of the SHWS pattern, x_i is the ith normalized pattern, $i = 1, 2, 3 \ldots$. We used MSE as the loss function and implement optimization with the Adam optimizer.[25] The MSE is calculated by

$$\mathrm{MSE}(y, y') = \frac{\sum_{i=1}^{N} y_i - y_i'}{N}, \tag{3}$$

where y_i is the ith ground truth of the Zernike mode coefficients, y_i' is the ith predicted result of the network, N is the number of the training datasets, $i = 1, 2, 3 \ldots$. Adaptive learning rate is utilized in the training, which starts from 0.1 and decreases with the iteration.

The convolutional neural network (CNN) we used here is mainly based on AlexNet, which is simple but effective in regression issues.[19,21,26] With the few parameters and layers, it could provide fast prediction speed, which is suitable for simplifying the distortion detection. The network we trained contains five convolutional layers and three dense (fully connected) layers, as shown in Fig. 2. The implementation environment is based on Keras with Tensorflow backend. The first two convolutional layers filter the inputted SHWS images with 32 kernels of size 5×5 and then followed by RELU operators and max pooling layers.[27,28] Each of the

Table 1. The coefficient ranges of 2nd ∼ 36th Zernike modes.

Modes	2nd–3rd	4th–6th	7th–10th	11th–15th	16th–21st	22nd–24th	25th–28th	29th–36th
Coefficients (rad)	±2	±5	±4	±3.2	±2.4	±2.1	±1.1	±0.6

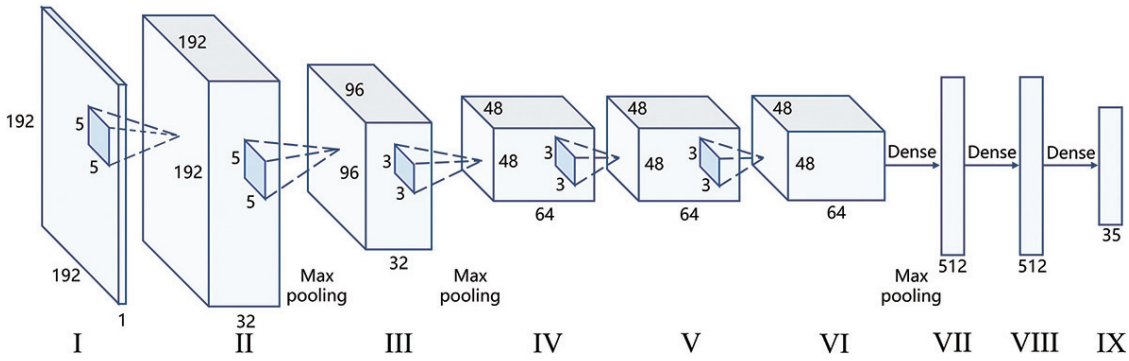

Fig. 2. The network architecture based on AlexNet. Layer I is the input pattern from SHWS; layer II–VI are convolutional layers and layer VII–IX are dense (fully connected) layers.

later three convolutional layers contains 64 kernels of size 3×3 and a RELU operator, and the fifth layer is followed by a max pooling layer. The next three fully connected layers have 512, 512 and 35 neurons, respectively. Each of the first two fully connected layers is followed by a RELU operator and the last layer is followed by a linear operator. The 35 parameters contained in the output layer IX refer to the predicted Zernike mode coefficients. Note that the first term of the Zernike mode named "piston" was not considered because it has no real effects on the overall wavefront distribution. In this simulation, the dataset generation and machine learning model training were completed on a personal computer (Intel Core i7 8700 3.2 GHz, Geil 16 GB DDR4, NVIDIA GeForce GTX 1060). Only one iteration was implemented to predict and correct the optical distortions.

In order to compare our method with the traditional methods, such as the modal-based SHWS, we reproduced the modal-based SHWS in simulation after referring to the previous work.[4]

3. Results and Discussions

The method proposed here is used to predict the Zernike mode coefficients of optical distortions directly from SHWS patterns. In order to simplify the wavefront sensing processes of SHWS, the Zernike mode coefficients of the optical distortions should be outputted while the trained model receives a full spot pattern from SHWS. That is, in the absence of complex wavefront calculation algorithms, only one trained model needs to be invoked to obtain the Zernike mode coefficients for wavefront reconstruction.

Figure 3 shows that the accuracy of the model increases with the number of epochs and tends to be saturated after the 20th epoch. After the model training, the testing datasets were inputted to the model for model prediction accuracy evaluation. To evaluate the distortion detection performance of our methods, we generated another 1024 datasets within the range given in Table 1 and repeated the detection. The repetition results show that the trained model obtained a coefficients detection accuracy up to 97.4%. Figure 4 provides the MSE of the predicted Zernike mode coefficients. The mean MSE of the predicted mode coefficients is 0.0014, which means that all distortions within the coefficient ranges can be accurately detected. The mean consumption time for each prediction is around 1.227 ms. It should be noted that, with a higher performance workstation, the prediction speed could be further improved. To further improve the

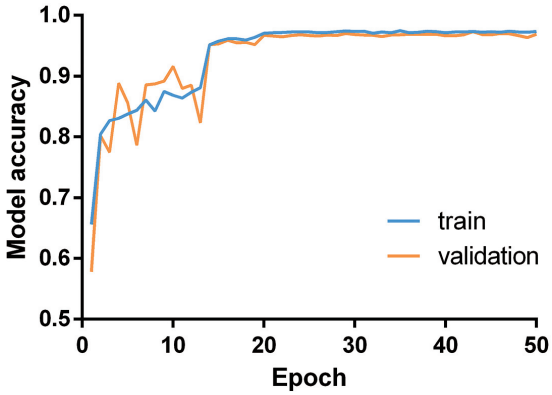

Fig. 3. The trend of model accuracy with the increase of epochs during the training. The accuracy of train datasets and validation datasets are indicated in blue and orange, respectively.

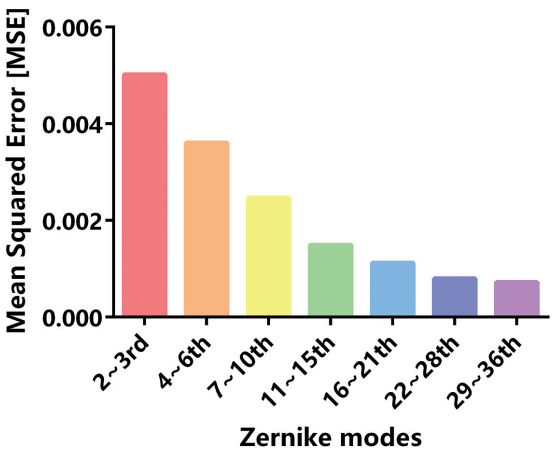

Fig. 4. The MSE of predicted Zernike mode coefficients.

accuracy of our method, it is preferred to use networks with deeper layers.

Four groups of model repetition verification results for distortions prediction and correction are shown in Fig. 5. Figure 5(a) records the spot patterns on the SHWS before (left) and after (right) correction. It can be found that our machine learning trained model can correct both serious and slight optical distortions. The amplitudes of the corresponding Zernike mode coefficients are shown in Fig. 5(b). The coefficient amplitudes predicted by the model (orange) are very close to the coefficient amplitudes of the loaded distortion (purple). Figure 5(c) illustrated the 3D wavefront distribution reconstructed from the predicted coefficients. From the distribution trend of optical distortions, it can be seen that the complexity of distortion detected by the model is higher than that of previous work, which means that our method can be used for rapid measurement of more serious distortions.[15]

To further investigate the optical distortions prediction capability of the trained model. We loaded the phase residuals after subtraction between original distortion and predicted distortion

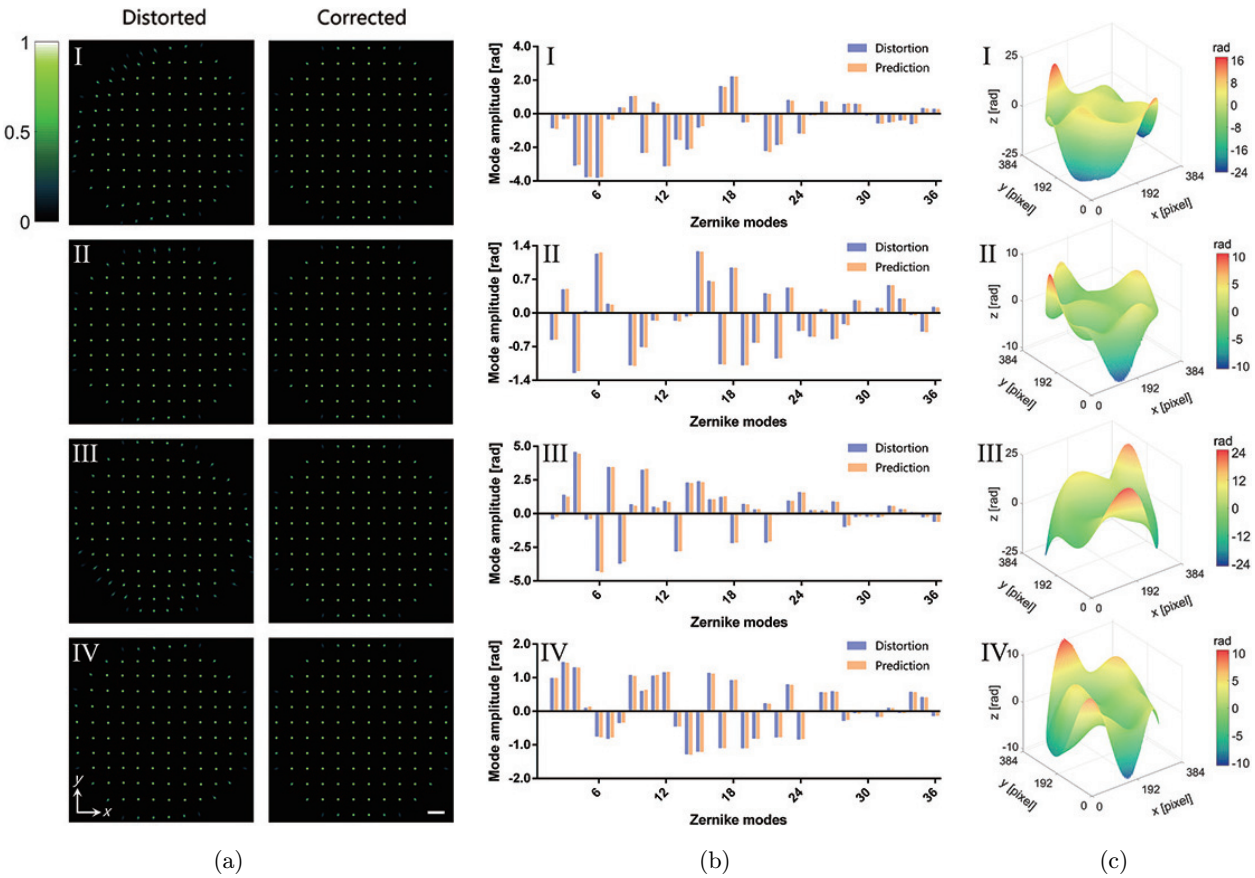

(a) (b) (c)

Fig. 5. Repeatability verification results for distortions prediction and correction. (a) The normalized intensity distribution of distorted spot patterns (left) and corrected spot patterns (right) captured on SHWS. The scale bar is 400 μm. (b) Amplitude comparison of 36 Zernike mode coefficients between distorted wavefront (purple) and predicted wavefront (orange). (c) 3D distribution of the predicted wavefront.

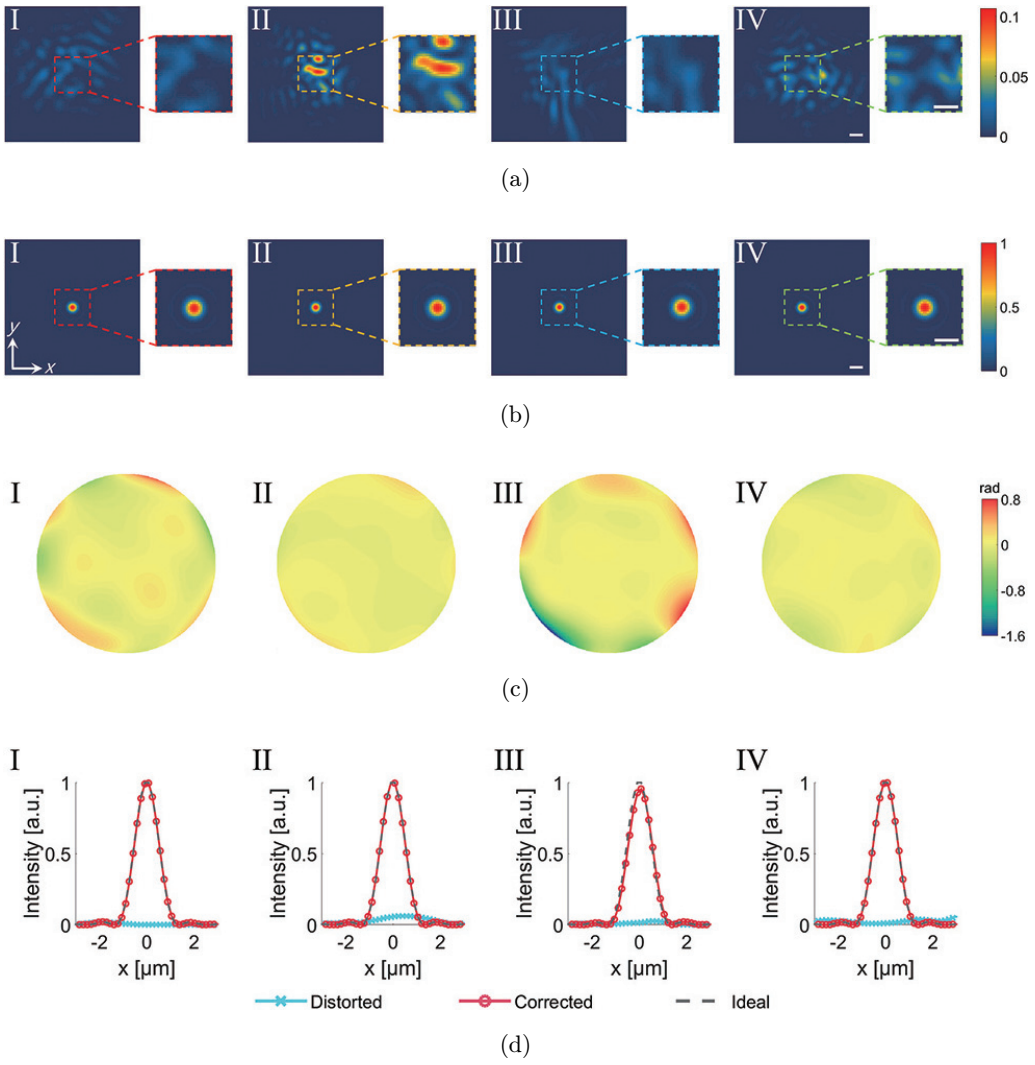

Fig. 6. The focusing results of optical distortions compensation from repetition tests. (a) The PSFs of the distorted wavefront. (b) The PSFs of the corrected wavefront. (c) The corrected wavefront after compensating with predicted Zernike mode coefficients. (d) Intensity distributions of PSFs in x-direction. The scale bar is 2 μm. The scale is the same in (a) and (b).

onto the SLM and recorded the corresponding PSFs to verify the correction effect of optical distortions. Figure 6 provides the intensity distributions of the PSFs corresponding to the verification data in Fig. 5. The distorted PSFs with added optical distortions are shown in Fig. 6(a). The intensity distributions in the central region are shown on the right side in the form of a subgraph. The corresponding wavefront compensation results of our model are provided in Fig. 6(b). Figure 6(c) lists the phase residuals loaded on the SLM after compensation. It can be seen that the compensated wavefront maintains a flat distribution, which means that the distortions are basically eliminated. The central intensity profiles of the ideal PSFs (without distortions), distorted PSFs and corrected PSFs in x-direction are compared in Fig. 6(d). It can be found that the central intensities of the PSFs are apparently enhanced after correction. Furthermore, the corrected PSFs have the similar profile distributions as the ideal PSFs, which means that the optical distortions are largely eliminated and the energy of the scattered light beam converges to the center again after correction.

It is necessary to examine the distortion detection performance of our method by comparing it with the traditional approaches. Here, we reproduced the modal-based SHWS and simulated the detection with 1024 datasets. The mean consumption time by modal approach for each detection is around 2.456 ms and the prediction speed of our method is 50.04% faster than the modal approach.

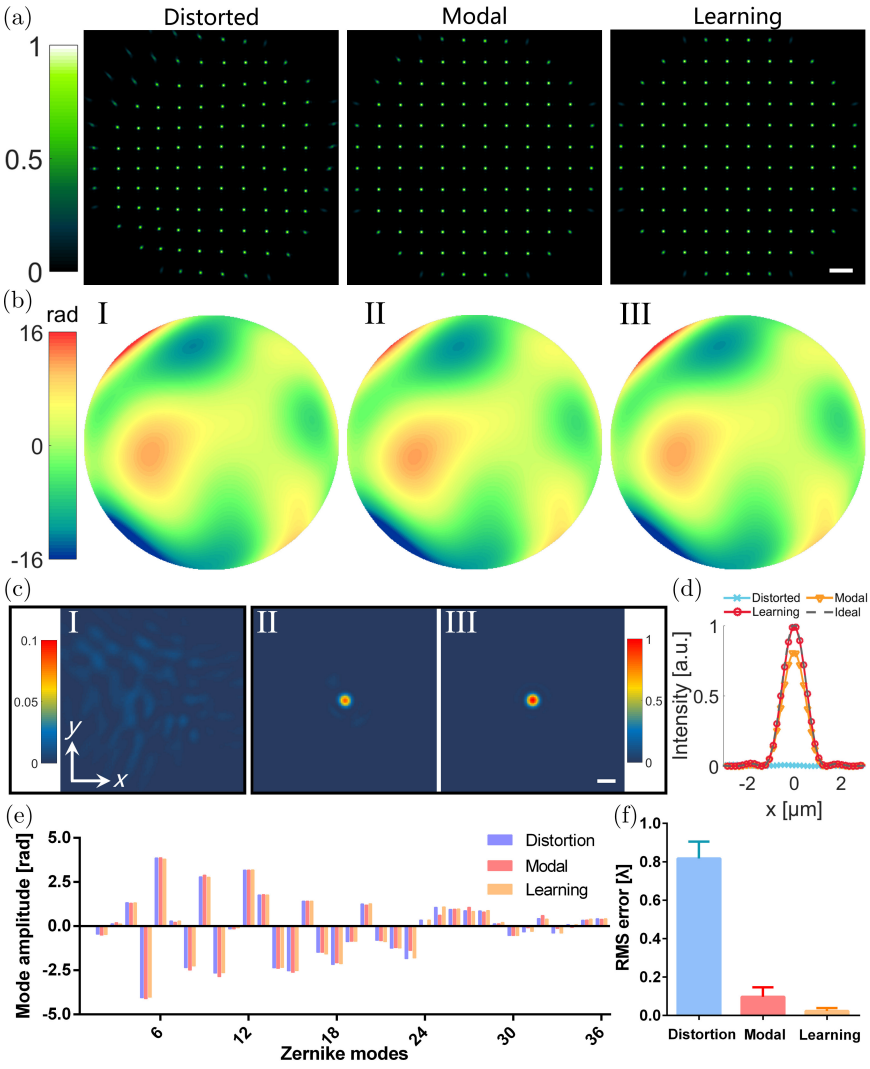

Fig. 7. Comparison of distortion detection results between modal-based method and our method. (a) The normalized intensity distribution of distorted spot pattern (left), the pattern corrected by modal approach (middle) and learning approach (right). The scale bar is 400 μm. (b) The original distortion "I", the distortion detected by modal approach "II" and the learning approach "III". (c) The intensity distributions of the distorted PSF "I", the PSF corrected by modal approach "II" and learning approach "III". The scale bar is 2 μm. (d) Intensity distributions of PSFs in x-direction. (e) The comparison of the Zernike mode coefficients. (f) The RMS error in phase residuals of 1024 datasets.

One group of comparison results of the distortion detection and compensation are shown in Fig. 7. From Fig. 7(a), we can find that both the modal approach and our method could correct the distorted SHWS pattern. However, the distortion at the edge of the pupil still exists in the pattern that corrected by modal approach. Figure 7(b) compares the original distortion with the two detected distortions. It is obvious that the distortion detected by our method is more close to the original one. To better compare the distortion correction results of these two methods, we simulated the PSFs before and after correction. Figure 7(c) gives the corresponding intensity distributions of the PSFs and the central profiles are shown in Fig. 7(d). After correcting with the wavefront detected by our method, the central profile of the PSF is close to the ideal one. Although the wavefront detected by modal approach could also correct the distorted PSF, there is still a gap between the focal intensity and the ideal one. The differences of Zernike mode coefficients shown in Fig. 7(e) provides a clear comparison between the two methods, where the coefficients of our method are more close to the modal approach. To quantitatively analyze the distortion detection performance of the two

methods, we calculated the root mean squared (RMS) error in phase residuals after wavefront compensation with the detected distortions. Figure 7(f) provides the RMS error of the distortion and the phase residuals. The RMS error of the distortion is $0.8173 \pm 0.0877\lambda$, the RMS error of the modal approach is $0.0969 \pm 0.0494\lambda$ and the RMS error of our method is $0.0236 \pm 0.0154\lambda$, which is 75.64% lower than that with modal approach.

4. Conclusion

In conclusion, to achieve *in vivo* high-resolution deep tissue imaging, a machine learning-based optical distortions detection method is proposed to simplify the wavefront sensing processes. Our results successfully demonstrate that the trained model has the capability to predict the distortion up to 36 Zernike modes in 1.227 ms with accuracy ~97.4%. During the wavefront detection, only one spot pattern from SHWS is required to predict the coefficients. The distortion detection speed of our method is 50.04% faster than the modal-based SHWS. After compensating with the wavefront predicted by our method, the average RMS error of phase residuals could be well decreased, and the RMS error of our method is 75.64% lower than that with modal-based SHWS. The simple detection process, high detection speed and the low RMS error substantially reduces the difficulty of wavefront detection based on SHWS. Therefore, this work has a potential significance to be applied in wavefront sensor-based AO for *in vivo* deep tissue imaging.

Conflict of Interest

The authors declare no conflicts of interest.

Acknowledgments

This work was supported by the National Natural Science Foundation of China (31571110, 61735016, 81771877), the Natural Science Foundation of Zhejiang Province of China (LZ17F050001), Zhejiang Lab (2018EB0ZX01) and the Fundamental Research Funds for the Central Universities.

References

1. N. Ji, "Adaptive optical fluorescence microscopy," *Nat. Methods* **14**(4), 374–380 (2017).
2. X. Zhu, Y. Xia, X. Wang, K. Si, W. Gong, "Optical brain imaging: A powerful tool for neuroscience," *Neurosci. Bull.* **33**(1), 95–102 (2017).
3. J. Primot, "Theoretical description of shack–hartmann wave-front sensor," *Opt. Commun.* **222**(1–6), 81–92 (2003).
4. G. Dai, *Wavefront Optics for Vision Correction*, Society of Photo-Optical Instrumentation Engineers (2008).
5. Y. Deng, J. Zhao, Y. Dai, Y. Zhang, "Simultaneous quantification of longitudinal and transverse ocular chromatic aberrations with hartmann–shack wavefront sensor," *J. Innov. Opt. Health Sci.* **11**(4), 1850021 (2018).
6. K. Wang, D. E. Milkie, A. Saxena, P. Engerer, T. Misgeld, M. E. Bronner, J. Mumm, E. Betzig, "Rapid adaptive optical recovery of optimal resolution over large volumes," *Nat. Methods* **11**(6), 625–628 (2014).
7. K. Wang, W. Sun, C. T. Richie, B. K. Harvey, E. Betzig, N. Ji, "Direct wavefront sensing for high-resolution in vivo imaging in scattering tissue," *Nat. Commun.* **6**, 7276 (2015).
8. R. Liu, Z. Li, J. S. Marvin, D. Kleinfeld, "Direct wavefront sensing enables functional imaging of infragranular axons and spines," *Nat. Methods* **16**(7), 615 (2019).
9. M. Cui, "Parallel wavefront optimization method for focusing light through random scattering media," *Opt. Lett.* **36**(6), 870–872 (2011).
10. C. Wang, R. Liu, D. E. Milkie, W. Z. Sun, Z. C. Tan, A. Kerlin, T. W. Chen, D. S. Kim, N. Ji, "Multiplexed aberration measurement for deep tissue imaging in vivo," *Nat. Methods* **11**(10), 1037–1040 (2014).
11. J. Yoon, M. Lee, K. Lee, N. Kim, J. M. Kim, J. Park, H. Yu, C. Choi, W. D. Heo, Y. Park, "Optogenetic control of cell signaling pathway through scattering skull using wavefront shaping," *Sci. Rep.* **5**, 13289 (2015).
12. J. Mompean, J. L. Aragon, P. M. Prieto, P. Artal, "Gpu-based processing of hartmann-shack images for accurate and high-speed ocular wavefront sensing," *Future Gener. Comput. Syst. Int. J. Esci.* **91**, 177–190 (2019).
13. M. Thier, R. Paris, T. Thurner, G. Schitter, "Low-latency shack–hartmann wavefront sensor based on an industrial smart camera," *IEEE Trans. Instrum. Meas.* **62**(5), 1241–1249 (2012).
14. Y. Rivenson, Z. Göröcs, H. Günaydin, Y. Zhang, H. Wang, A. Ozcan, "Deep learning microscopy," *Optica* **4**(11), 1437–1443 (2017).
15. E. Nehme, L. E. Weiss, T. Michaeli, Y. Shechtman, "Deep-storm: Super-resolution single-molecule microscopy by deep learning," *Optica* **5**(4), 458–464 (2018).

16. S. Cheng, H. Li, Y. Luo, Y. Zheng, P. Lai, "Artificial intelligence-assisted light control and computational imaging through scattering media," *J. Innov. Opt. Health Sci.* **12**(4), 1930006 (2019).
17. C. Ahn, B. Hwang, K. Nam, H. Jin, T. Woo, J.-H. Park, "Overcoming the penetration depth limit in optical microscopy: Adaptive optics and wavefront shaping," *J. Innov. Opt. Health Sci.* **12**(4), 1930002 (2019).
18. S. W. Paine, J. R. Fienup, "Machine learning for improved image-based wavefront sensing," *Opt. Lett.* **43**(6), 1235–1238 (2018).
19. Y. Jin, Y. Zhang, L. Hu, H. Huang, Q. Xu, X. Zhu, L. Huang, Y. Zheng, H. L. Shen, W. Gong, K. Si, "Machine learning guided rapid focusing with sensor-less aberration corrections," *Opt. Express* **26**(23), 30162–30171 (2018).
20. Y. Nishizaki, M. Valdivia, R. Horisaki, K. Kitaguchi, M. Saito, J. Tanida, E. Vera, "Deep learning wavefront sensing," *Opt. Express* **27**(1), 240–251 (2019).
21. Y. Zhang, C. Wu, Y. Song, K. Si, Y. Zheng, L. Hu, J. Chen, L. Tang, W. Gong, "Machine learning based adaptive optics for doughnut-shaped beam," *Opt. Express* **27**(12), 16871–16881 (2019).
22. H. Guo, N. Korablinova, Q. S. Ren, J. Bille, "Wavefront reconstruction with artificial neural networks," *Opt. Express* **14**(14), 6456–6462 (2006).
23. Z. Q. Li, X. Y. Li, "Centroid computation for shack-hartmann wavefront sensor in extreme situations based on artificial neural networks," *Opt. Express* **26**(24), 31675–31692 (2018).
24. M. A. A. Neil, M. J. Booth, T. Wilson, "Closed-loop aberration correction by use of a modal zernike wave-front sensor," *Opt. Lett.* **25**(15), 1083–1085 (2000).
25. D. Kingma, J. Ba, "Adam: A method for stochastic optimization," https://arxiv.org/abs/1412.6980 (2014).
26. A. Krizhevsky, I. Sutskever, G. E. Hinton, "Imagenet classification with deep convolutional neural networks," in *Int. Conf. Neural Information Processing Systems*, pp. 1097–1105, Curran Associates, Inc. (2012).
27. K. Hara, D. Saito, H. Shouno, "Analysis of function of rectified linear unit used in deep learning," *2015 Int. Joint Conf. Neural Networks (IJCNN)*, pp. 1–8, Killarney, Ireland (2015).
28. B. Graham, "Fractional max-pooling, https://arxiv.org/abs/1412.6071 (2014).